Supplementary information

Imaging cardiomyocyte beating

We evaluated compressed FLIM in imaging MacQ-mOrange2 to detect beating in cultured rat heart cardiomyocytes. We transfected cardiomyocytes with plasmid DNA MacQ-mOrange2 and stimulated with acetylcholine. As an example, the induced fluorescence intensity oscillation is shown in **Fig. S6**. We then used compressed FLIM to image the cardiomyocyte beating. **Fig. S7b** shows the fluorescence intensity and lifetime traces of MacQ-mOrange2 sensor expressed in a cultured cardiomyocyte with acetylcholine stimulation imaged at 40 Hz. **Movie S5** records the lifetime dynamics due to cardiomyocyte beating. Representative snapshots at 216 ms, 513 ms, 621 ms, 810 ms, 1080 ms and 1512 ms are shown in **Fig. S7c**. The average relative fluorescence intensity change ($\Delta F/F$) and absolute lifetime change ($\Delta\tau$) in response to one beating event is -1.2% and -0.2 ns. respectively. Finally, to provide a negative control, we imaged MacQ-mOrange2 without acetylcholine stimulation (**Fig. S7d**). Both the fluorescence intensities and lifetimes were stable during the entire time trace, and no beatings were observed.

Myocytes transfection

We used Mac mutant plasmid DNA Mac-mOrange2 (#48761, Addgene) to transfect the rat heart cardiomyocytes 10 DIV (H9c2(2-1) ATCC® CRL-1446™), and lipofectamine 2000 (Invitrogen) was used as the transfecting reagent. We imaged the rat heart cardiomyocytes 2 days after transfection. We used acetylcholine to stimulate cardiomyocyte beating. The base medium for this cell line was Dulbecco's Modified Eagle's Medium (#30-2002, ATCC). At each stimulation, we removed the media in the plate and pipetted fresh medium containing 100μM acetylcholine to cardiomyocytes[1].

Imaging hematoxylin and eosin (H&E) stained tissue slide

We further validated compressed FLIM in imaging a hematoxylin and eosin (H&E) stained tissue slide. In the sample, we stained connective tissues and extracellular materials using fluorophore eosin. We excited the sample at 515 nm, and imaged the fluorescence using a ×60 1.42 NA oil immersion objective lens (PLAPON 60XO, Olympus). The fluorescence intensity and reconstructed lifetime images are shown in **Fig. S8a** and **S8b**, respectively. The observed fluorescence lifetime heterogeneity in **Fig. S8b** is attributed to eosin quenching[2]. To validate our results, we imaged the sample using a line-scanning streak camera imaging approach (Methods). The ground-truth image is shown in **Fig. S8c**, matching well with compressed FLIM measurement.

Compressed spectral FLIM (sFLIM) imaging

In fluorescence microscopy, multi-target imaging is commonly accomplished by means of spectrally resolved detection and multicolor analysis[3–5] or time-resolved detection by FLIM[6–7]. However, given a single measurement dimension (spectrum or time), the fluorescence characteristics of co-located fluorophores must differ substantially in order for them to be separated, a fact which limits the number of fluorophores that can be simultaneously imaged. Taking the full advantages of spectral and temporal characteristics of a fluorophore can relieve this requirement and significantly improve the accuracy of unmixing[8]. Herein we expanded the functionality of compressed FLIM to color reproduction and demonstrated compressed spectral FLIM (sFLIM) in imaging multi-target fluorescence samples.

The compressed sFLIM system is shown in **Fig. S9a**. We inserted a bandpass filter in each of two temporally-sheared imaging channels and selectively passed light at given wavelengths: orange (ET590/50m, Chroma) and near infrared (ET690/50m, Chroma). Accordingly, we changed the emission filter of the microscope to a multi-bandpass filter (59007m, Chroma). The resultant temporally-sheared channels record the fluorescence scene filtered at two different wavelengths. To reconstruct the sFLIM image, we separately computed the lifetime images at these two wavelengths using the single-channel TwIST algorithm and registered their images thereafter.

Compared with using lifetime or spectral information alone, the combination of multidimensional fluorescence data can significantly improve the accuracy of fluorophore decomposition. We adopted a previously described algorithm[8,9] to process the multidimensional data acquired by compressed sFLIM. A probability function $p(t,\lambda)dtd\lambda$, referred to as fluorescence pattern, is constructed to describe how many photons per time interval dt and per spectral bandwidth $d\lambda$ are expected from a given fluorophore. At each spatial pixel, the light intensity that compressed sFLIM measures is the superposition of individual fluorescence patterns:

$$\begin{aligned}\tilde{I}(t,\lambda_1)dtd\lambda &= \sum_i c_i p_i(t,\lambda_1)dtd\lambda \\ \tilde{I}(t,\lambda_2)dtd\lambda &= \sum_i c_i p_i(t,\lambda_2)dtd\lambda\,.\end{aligned} \tag{1}$$

Here, λ_1 and λ_2 are the corresponding peak emission wavelengths in two spectral channels, and c_i denotes the concentration of fluorophore i. Decomposition of fluorophores at a given spatial pixel (i.e., calculation of c_i) is the solution of the inverse problem of Eq. 1.

The numerical solution of this problem can be found by minimizing the Kullback-Leibler discrepancy Δ_{KL}:

$$\Delta_{KL} = \sum_{t,\lambda} \tilde{I}(t,\lambda) - \hat{I}(t,\lambda) + \hat{I}(t,\lambda)\left[\ln \hat{I}(t,\lambda) - \ln \tilde{I}(t,\lambda)\right], \quad (2)$$

where $\hat{I}(t,\lambda)$ is the estimation that is calculated by $\hat{I}(t,\lambda) = \sum_i \hat{c}_i p_i(t,\lambda)$. A positively constrained solution (i.e., $\hat{c}_i > 0$ for all i) of Eq. 2 can be found via a typical non-negative matrix factorization algorithm[10]. In brief, the algorithm starts with a reasonably estimated positive concentration vector $\hat{\boldsymbol{c}}$ and determines the local gradient. During iteration, the concentration vector is updated such a way that it can be expressed as the multiplication with a positively constrained scaling vector $\boldsymbol{\gamma}$: $\hat{\boldsymbol{c}}_{n+1} = \boldsymbol{\gamma}\hat{\boldsymbol{c}}_n$.

To demonstrate sFLIM, we imaged a mixture of fluorescent beads with varied lifetimes or emission spectra (6 um diameter orange, F8825; 15 um diameter orange, F8841; 10 um diameter crimson F8831; Thermo Fisher). The fluorescence lifetime and spectral data of these beads are shown in **Fig. S9b** and **Fig. S9c**, respectively. Within a snapshot, we captured the spectrally-resolved lifetime images and show them in **Fig. S9d**. Moreover, we applied the spectral-lifetime unmixing algorithm to the dataset and separated these beads in individual channels as shown in **Fig. S9e**.

Comparison of encoding strategies

Given an object function $f \in \mathbb{R}^N$ containing k non-zero values, we perform M linear measurements $y \in \mathbb{R}^M$ by applying a sensing matrix $\Phi \in \mathbb{R}^{M\times N}$ to f:

$$y = \Phi f. \quad (3)$$

Provided that k < M << N, the object function can be reasonably estimated through compressed sensing. The error ε between the reconstructed signal $\hat{f}$ and the original signal f can be calculated as[11]:

$$\varepsilon = \left\| f - \hat{f} \right\|_{l_2} \leq C_{p,\alpha} \cdot R \cdot \left(\frac{M}{\log N}\right)^{-r}, \quad r = \frac{1}{p} - \frac{1}{2}, \quad (4)$$

where $0 < p \leq 1$, and $C_{p,\alpha}$ and R are constants. Equation 4 implies that a larger M leads to a smaller ε.

Next, we compare three encoding strategies: single-channel encoding, complementary dual-channel encoding, and complementary dual-channel encoding with a reference image constraint. The corresponding forward models are:

$$E_{C_1} = TSC_1 I, \quad (5)$$

$$\begin{bmatrix} E_{C_1} \\ E_{C_2} \end{bmatrix} = \begin{bmatrix} TSC_1 \\ TSC_2 \end{bmatrix} I, \tag{6}$$

and

$$\begin{bmatrix} E_I \\ E_{C_1} \\ E_{C_2} \end{bmatrix} = \begin{bmatrix} T \\ TSC_1 \\ TSC_2 \end{bmatrix} I, \tag{7}$$

where the measurement $y \in \mathbb{R}^1$, $\mathbb{R}^2$, and $\mathbb{R}^3$, respectively. Therefore, the complementary dual-channel encoding with a reference image constraint provides the smallest error ε and thereby the highest reconstructed image quality.

To quantitatively show this advantage, we imaged a fluorescent tissue paper and compared the results using the three encoding strategies (**Fig. S10**). The PSNR (peak signal to noise ratio) of the resultant images are 14 dB, 17 dB, and 25 dB, respectively. Echoing the theoretical analysis, the dual-channel encoding with a reference image constraint provides the best image quality.

In compressed FLIM, we used a random, binary pattern for spatial encoding. The rationale is that the correspondent operators C_1, C_2 have low coherence with any representation basis[12] and low coherence between their normalized columns[13-15], and are generally applicable to natural scenes, making it a common choice for compressed imaging[16-19].

Imaging parameters of the experiments performed

We summarized $N_{y\prime}$, N_y, N_t, CR, and the streak camera's observation time window T used in all experiments in **Table 2** below.

Experiments	$N_{y\prime}$	N_y	N_t	CR	T
Imaging of fluorescent beads	688	189	500	69	20 ns
Imaging of neural cytoskeletal proteins	599	400	200	67	100 ns
Imaging of neural spikes-FRET	399	200	200	50	50 ns
Imaging of neural spikes-neural spikes	499	200	300	60	20 ns

Table 2: Imaging parameters. $N_{y\prime}$, total number of detector rows of the camera; N_y, number of spatial samplings along the y axis of the event datacube; N_t, temporal sequence depth; CR, compression ratio; T, streak camera's observation time window.

Reference

1. Vianney, John-Mary, Damon A. Miller, and John M. Spitsbergen. "Effects of acetylcholine and electrical stimulation on glial cell line-derived neurotrophic factor production in skeletal muscle cells." Brain research 1588 (2014): 47-54.
2. Luo, Teng, et al. "Multiplexed fluorescence lifetime imaging by concentration-dependent quenching." Journal of Materials Chemistry B 6.13 (2018): 1912-1919.

3. Liyanage, M. et al. Multicolour spectral karyotyping of mouse chromosomes. Nat. Genet. 14, 312– 315 (1996).
4. Garini, Y., Gil, A., Bar-Am, I., Cabib, D. & Katzir, N. Signal to noise analysis of multiple color fluorescence imaging microscopy. Cytometry 35, 214–226 (1999).
5. Tsurui, H. et al. Seven-color fluorescence imaging of tissue samples based on Fourier spectroscopy and singular value decomposition. J. Histochem. Cytochem. 48, 653–662 (2000).
6. Bastiaens, P.I. & Squire, A. Fluorescence lifetime imaging microscopy: spatial resolution of biochemical processes in the cell. Trends Cell Biol. 9, 48–52 (1999).
7. Chang, C.W., Sud, D. & Mycek, M.A. Fluorescence lifetime imaging microscopy. Methods Cell Biol. 81, 495–524 (2007).
8. Niehörster, Thomas, et al. "Multi-target spectrally resolved fluorescence lifetime imaging microscopy." Nature methods13.3 (2016): 257.
9. I. Gregor, M. Patting, Pattern-based linear unmixing for efficient and reliable analysis of multicomponent TCSPC data, Advanced Photon Counting, Springer, 2014, pp. 241-263.
10. D.D. Lee, H.S. Seung, Algorithms for non-negative matrix factorization, in: Advances in neural information processing systems, 2001, pp. 556-562.
11. E. J. Candes and T. Tao, "Near-Optimal Signal Recovery From Random Projections: Universal Encoding Strategies?" in IEEE Transactions on Information Theory, vol. 52, no. 12, pp. 5406-5425, Dec. 2006.
12. Candès, Emmanuel J., and Michael B. Wakin. "An introduction to compressive sampling." *IEEE signal processing magazine* 25.2 (2008): 21-30.
13. M. F. Duarte and Y. C. Eldar, “Structured compressed sensing: from theory to applications,” IEEE Trans. Signal Process. 59, 4053–4085 (2011).
14. E. J. Cands and J. Romberg, “Sparsity and incoherence in compressive sampling,” Inverse Probl. 23, 969–985 (2007).
15. L. Carin, D. Liu, and B. Guo, “Coherence, compressive sensing, and random sensor arrays,” IEEE Antennas Propag. Mag. 53(4), 28–39 (2011)
16. W. Lu, T. Dai and S. Xia, "Binary Matrices for Compressed Sensing," in IEEE Transactions on Signal Processing, vol. 66, no. 1, pp. 77-85, 1 Jan.1, 2018, doi: 10.1109/TSP.2017.2757915.
17. Amini, Arash, and Farokh Marvasti. "Deterministic construction of binary, bipolar, and ternary compressed sensing matrices." IEEE Transactions on Information Theory 57.4 (2011): 2360-2370.
18. Zhang, Gesen, et al. "Compressed sensing and reconstruction with bernoulli matrices." The 2010 IEEE International Conference on Information and Automation. IEEE, 2010.
19. Oktem, Figen S., Liang Gao, and Farzad Kamalabadi. “Computational Spectral and Ultrafast Imaging via Convex Optimization.” Handbook of Convex Optimization Methods in Imaging Science. Springer, Cham, 2017. 105-127

Video legends:

Movie S1. Compressed FLIM system in action

Movie S2. Reconstructed fluorescence beads flow dynamics by compressed FLIM

Movie S3. Reconstructed time-lapse fluorescence decay process of immunofluorescently-stained neurons after a single pulse excitation by compressed FLIM

Movie S4. Reconstructed lifetime dynamics due to neural pulsing by compressed FLIM

Movie S5. Reconstructed lifetime dynamics due to cardiomyocyte beating by compressed FLIM

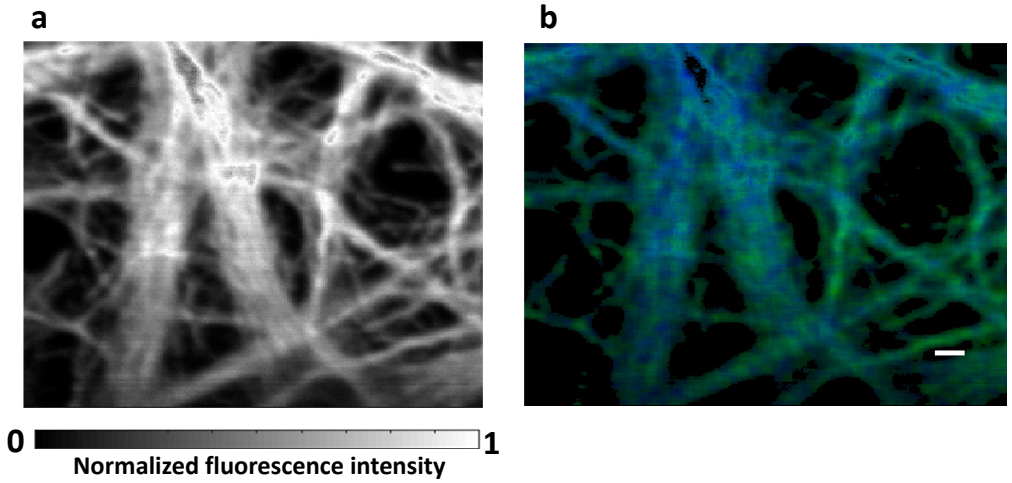

Fig.S1

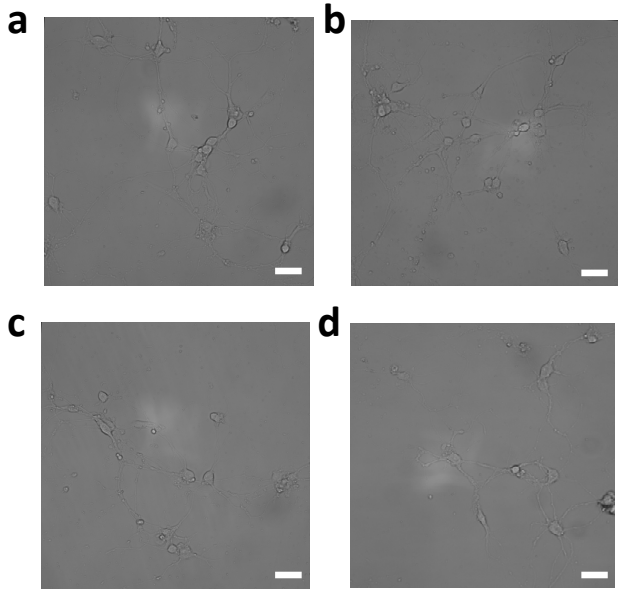

Fig.S2

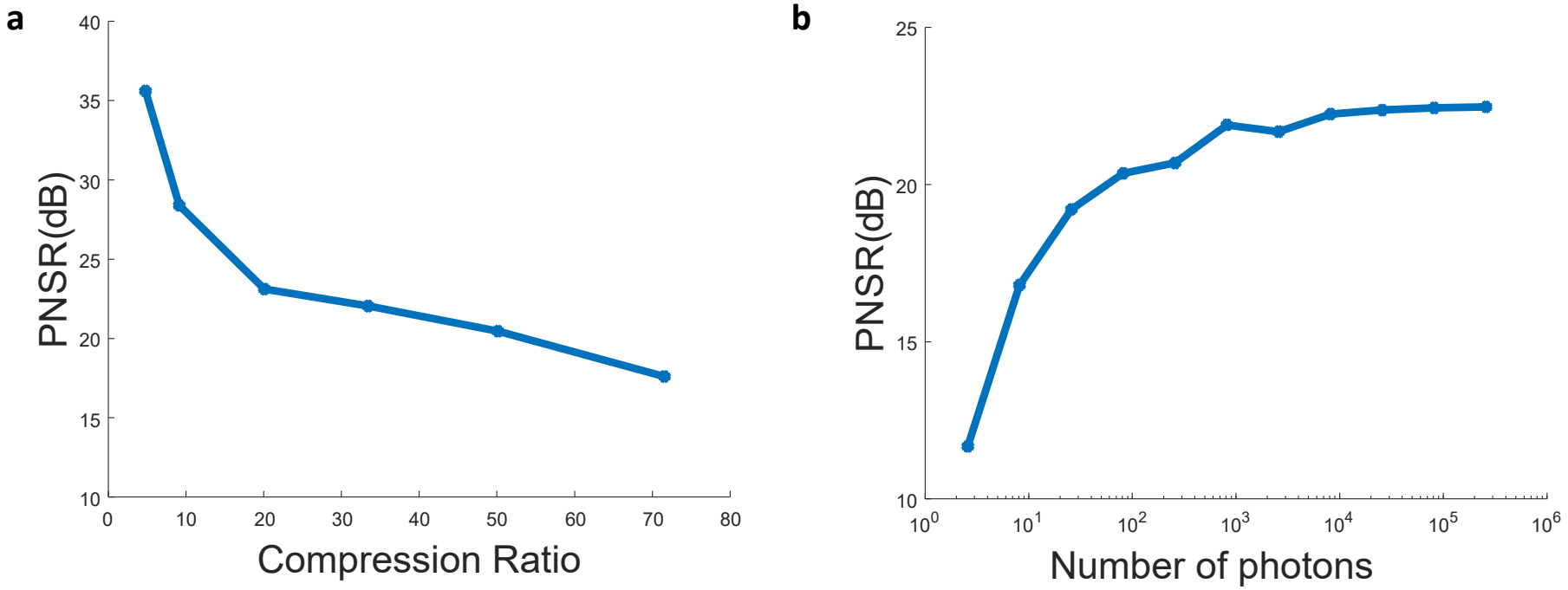

Fig.S3

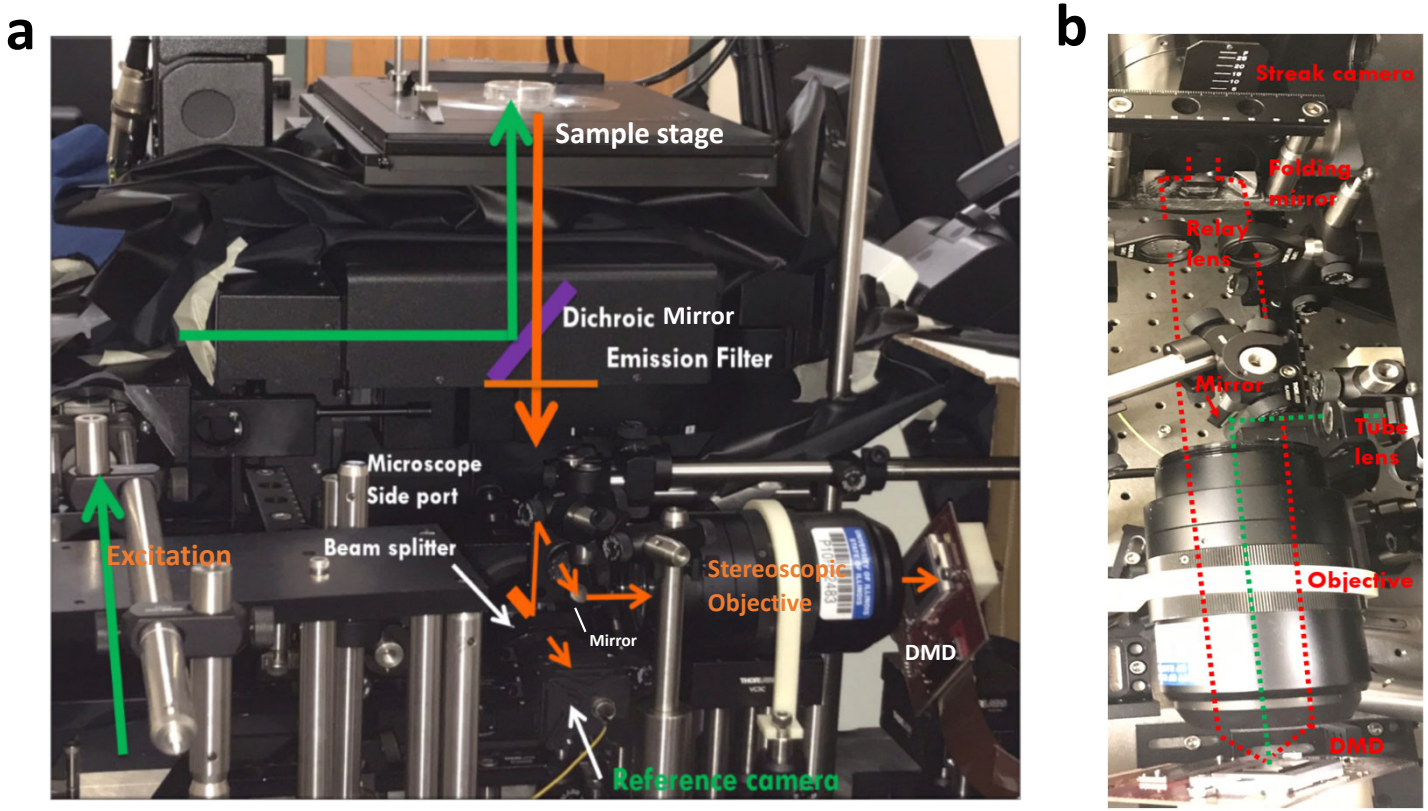
a
Sample stage
Dichroic Mirror
Emission Filter
Microscope
Side port
Excitation
Beam splitter
Stereoscopic
Objective
Mirror
DMD
Reference camera
b
Streak camera
Folding
mirror
Relay
lens
Mirror
Tube
lens
Objective
DMD

Fig.S4

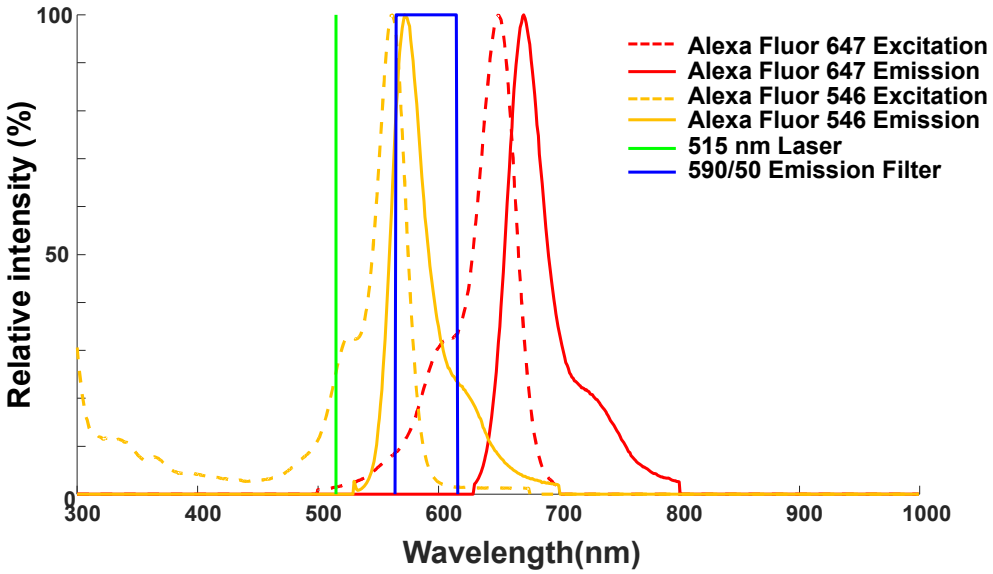
Alexa Fluor 647 Excitation
Alexa Fluor 647 Emission
Alexa Fluor 546 Excitation
Alexa Fluor 546 Emission
515 nm Laser
590/50 Emission Filter
Relative intensity (%)
100
50
0
300
400
500
600
700
800
900
1000
Wavelength(nm)

Fig.S5

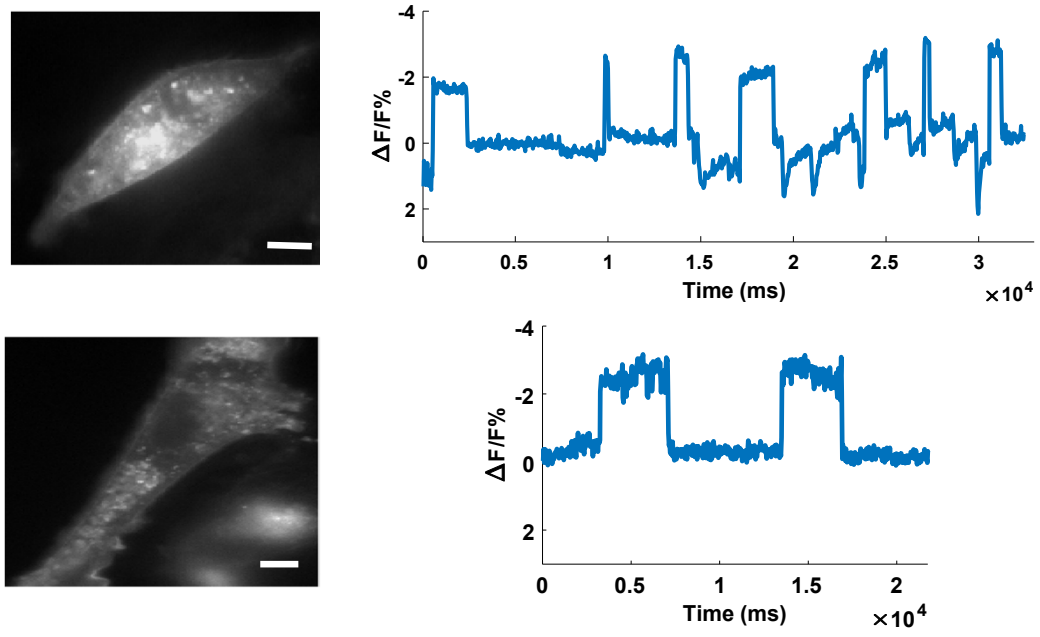

Fig.S6

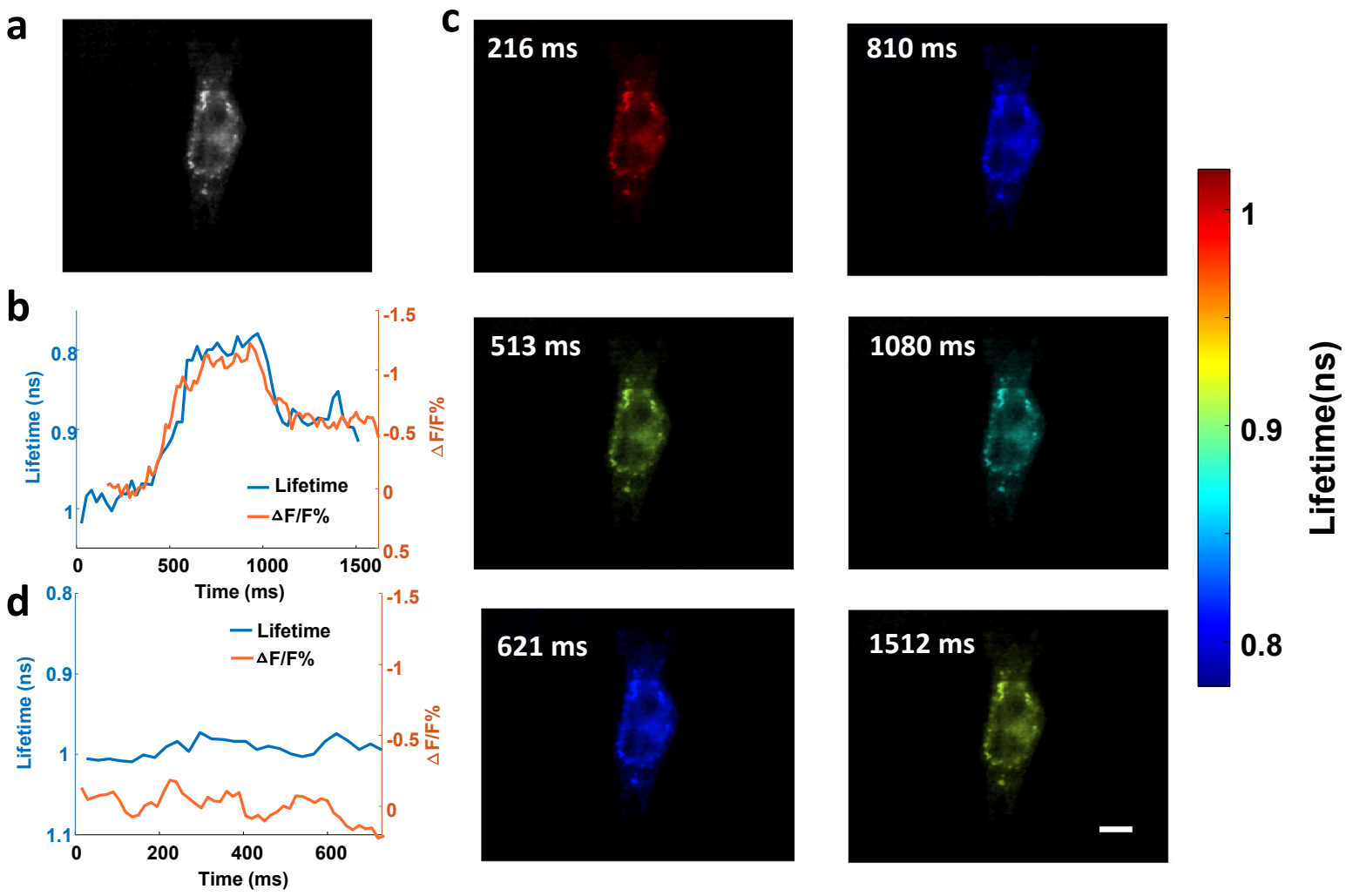
a
b
c
d
216 ms
810 ms
513 ms
1080 ms
621 ms
1512 ms
Lifetime(ns)
1
0.9
0.8
Lifetime (ns)
ΔF/F%
Lifetime
ΔF/F%
Time (ms)
0.8
0.9
1
1.1
-1.5
-1
-0.5
0
0.5
0
500
1000
1500
200
400
600

Fig.S7

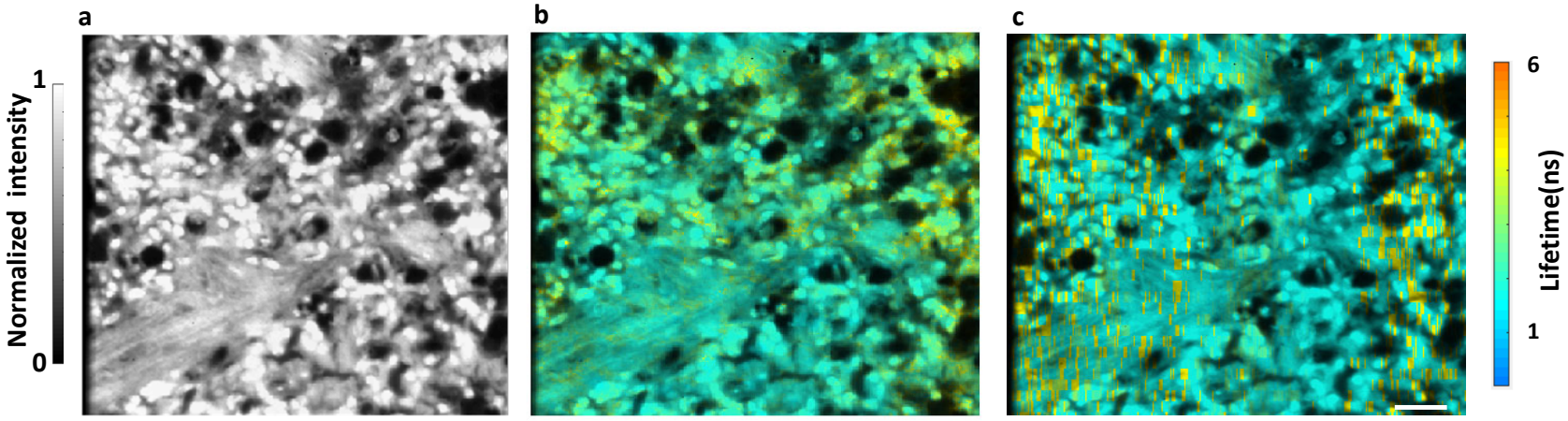

Fig.S8

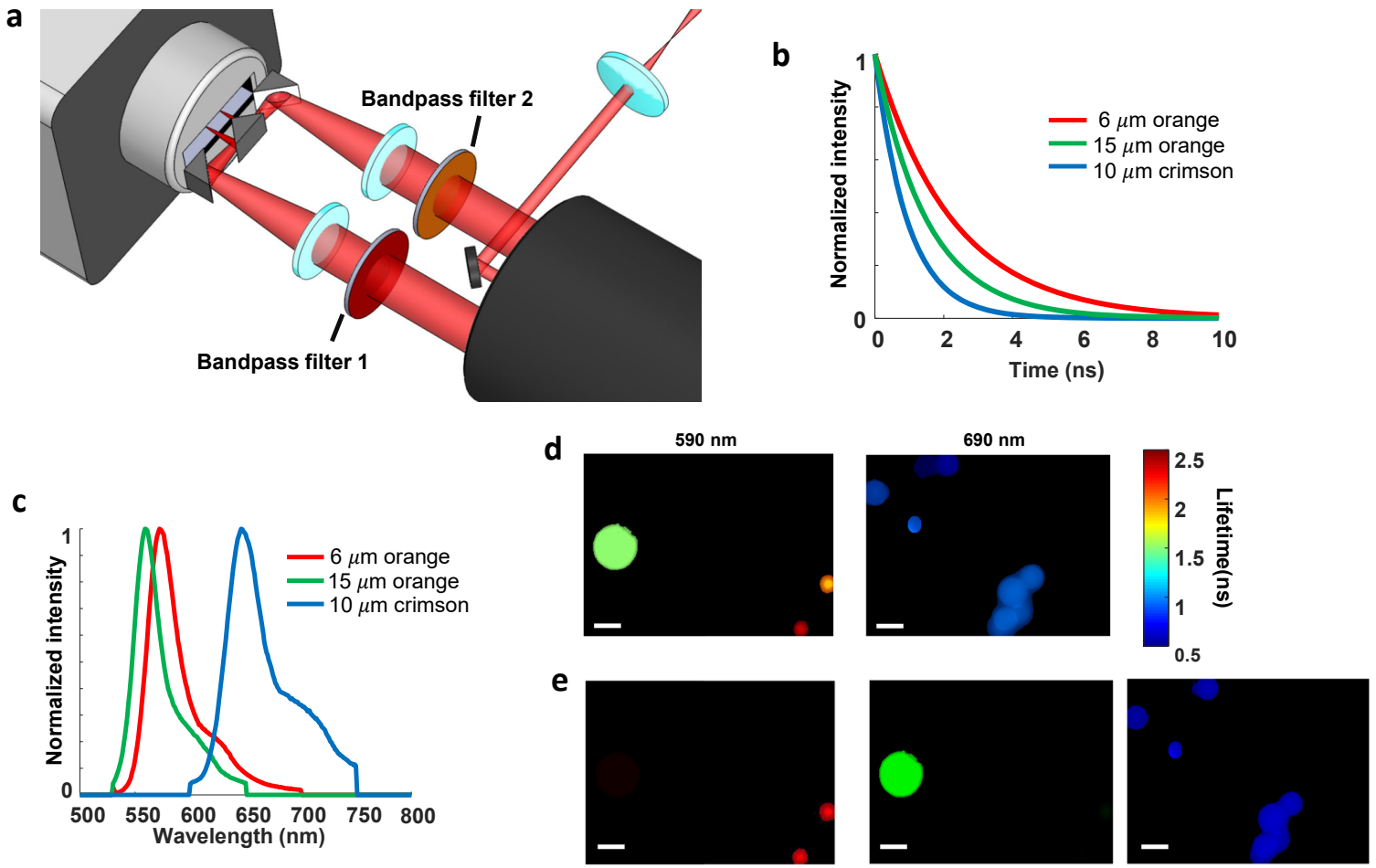
a
Bandpass filter 2
Bandpass filter 1
b
Normalized intensity
1
0
0
2
4
6
8
10
Time (ns)
6 μm orange
15 μm orange
10 μm crimson
c
Normalized intensity
1
0
500
550
600
650
700
750
800
Wavelength (nm)
6 μm orange
15 μm orange
10 μm crimson
d
590 nm
690 nm
2.5
2
1.5
1
0.5
Lifetime(ns)
e

Fig.S9

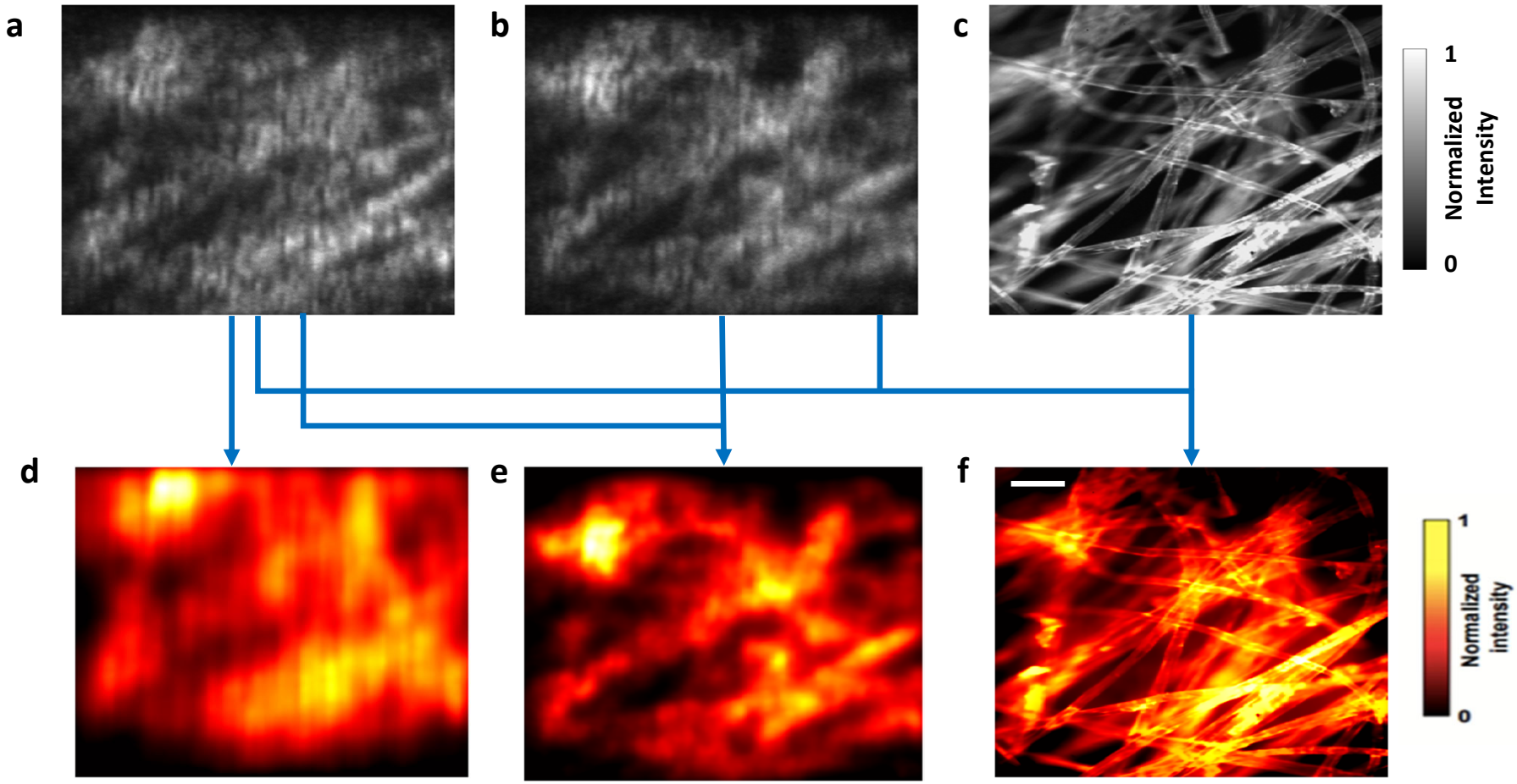

Fig.S10